AD-A066 541 CALIFORNIA UNIV IRVINE DEPT OF PHYSICS F/G 20/9
SURFACE PLASMA WAVES IN SILVER AND GOLD.(U)
1976 P FERGUSON, R F WALLIS, M BELAKHOVSKY N00014-76-C-0121
UNCLASSIFIED NL

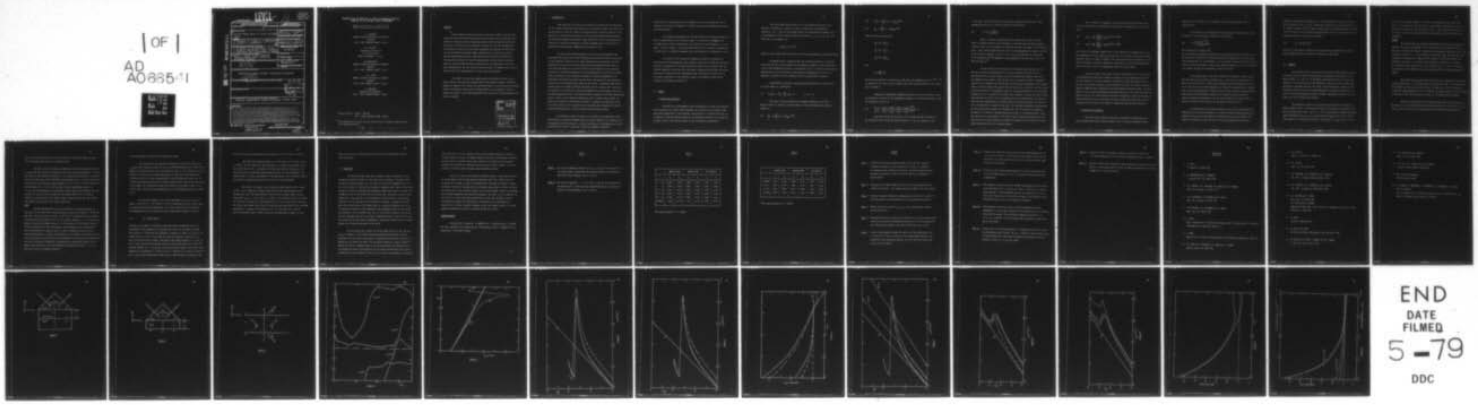

END
DATE FILMED
5-79
DDC

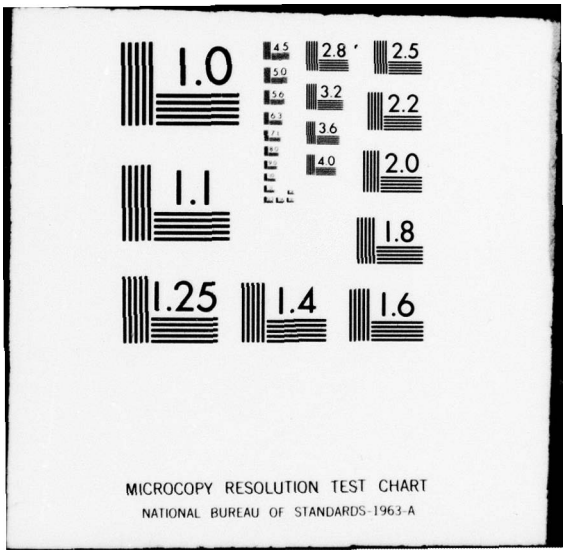
1.0
1.1
1.25
1.4
1.6
1.8
2.0
2.2
2.5
2.8
3.2
3.6
4.0
4.5
5.0
5.6
6.3
MICROCOPY RESOLUTION TEST CHART
NATIONAL BUREAU OF STANDARDS-1963-A

LEVEL II

392-001
LF
4/21/78

UNCLASSIFIED

SECURITY CLASSIFICATION OF THIS PAGE (When Data Entered)

REPORT DOCUMENTATION PAGE

READ INSTRUCTIONS BEFORE COMPLETING FORM

1. REPORT NUMBER
2. GOVT ACCESSION NO.
3. RECIPIENT'S CATALOG NUMBER

4. TITLE (and Subtitle)
Surface Plasma Waves in Silver and Gold

5. TYPE OF REPORT & PERIOD COVERED
Interim rept.

6. PERFORMING ORG. REPORT NUMBER

7. AUTHOR(s)
P. Ferguson, R. F. Wallis, M. Belakhovsky
J. P. Jadot, J. Tomkinson

8. CONTRACT OR GRANT NUMBER(s)
N00014-76-C-0121

9. PERFORMING ORGANIZATION NAME AND ADDRESS
R. F. Wallis, U. of California, Irvine
P. Ferguson, Belakhovsky, Jadot, Grenoble
J. Tomkinson, Inst. Laue-Langevin, Grenoble

10. PROGRAM ELEMENT, PROJECT, TASK AREA & WORK UNIT NUMBERS
NR 392-001

11. CONTROLLING OFFICE NAME AND ADDRESS
R Wallis - Office of Naval Research
Physics Program, 800 N. Quincy St.
Arlington, VA 22217

12. REPORT DATE
1976

13. NUMBER OF PAGES
38

14. MONITORING AGENCY NAME & ADDRESS (if different from Controlling Office)

15. SECURITY CLASS. (of this report)
UNCLASSIFIED

15a. DECLASSIFICATION/DOWNGRADING SCHEDULE

16. DISTRIBUTION STATEMENT (of this Report)
Approved for public release; distribution unlimited

39p.

17. DISTRIBUTION STATEMENT (of the abstract entered in Block 20, if different from Report)

18. SUPPLEMENTARY NOTES

19. KEY WORDS (Continue on reverse side if necessary and identify by block number)
Surfaces, Plasma Waves, Surface Polaritons, Silver, Gold

Abstract

The dispersion curves for surface plasma waves (SPW) in Ag have been determined from calculated reflectivity minima as exhibited by attenuated total reflection (ATR spectra) for the prism-air-metal (PAM) configuration and from the direct calculation of the dispersion relation for the same configuration. The dispersion curves for Au have been determined by mensuring the ATR spectra for the prism-dielectric-metal (PDM) configuration, by calculating the ATR spectra from published optical constants and from the direct calculation of the dispersion relation for the PDM configuration. We have found two general types of solutions from the direct calculation of the dispersion relation for both configurations. The two solutions are the surface or Brewster modes and the virtual modes. The characteristics of both modes are discussed.

The effect of electronic damping upon the dispersion curves for AG which exhibits low electronic damping and Au which exhibits moderate electronic damping is demonstrated. Finally the perturbing effect of the dielectric (referred herein as dielectric shift) upon the displacement of the dispersion curves to higher wave number for the PAM configuration for Ag and for the PDM configuration for Au is shown.

DD FORM 1 JAN 73 1473 EDITION OF 1 NOV 65 IS OBSOLETE
S/N 0102-LF-014-6601

UNCLASSIFIED
SECURITY CLASSIFICATION OF THIS PAGE (When Data Entered)

403659

SURFACE PLASMA WAVES IN SILVER AND GOLD

P. FERGUSON*
CENTRE d'ETUDES NUCLEAIRES de GRENOBLE
LETI/EPA
85 X - 38041 GRENOBLE CEDEX - France

R.F. WALLIS***
Department of Physics
U. of California
IRVINE, CALIFORNIA - U.S.A.

M. BELAKHOVSKY
CENTRE d'ETUDES NUCLEAIRES de GRENOBLE
DRF/CPN
85 X - 38041 GRENOBLE CEDEX - France

J.P. JADOT
CENTRE d'ETUDES NUCLEAIRES de GRENOBLE
LETI/EPA
85 X - 38041 GRENOBLE CEDEX - France

J. TOMKINSON
INSTITUTE LAUE-LANGEVIN
156 X - 38041 GRENOBLE CEDEX - France

* Present address : CEN.G - DRF/CPN
85 X - 38041 GRENOBLE CEDEX, France.

*** Work supported in part by the U.S. Office of Naval Research under Contract No. N 00014-76-C-0121.

ABSTRACT

The dispersion curves for surface plasma waves (SPW) in Ag have been determined from calculated reflectivity minima as exhibited by attenuated total reflection (ATR spectra) for the prism-air-metal (PAM) configuration and from the direct calculation of the dispersion relation for the same configuration. The dispersion curves for Au have been determined by measuring the ATR spectra for the prism-dielectric-metal (PDM) configuration, by calculating the ATR spectra from published optical constants and from the direct calculation of the dispersion relation for the PDM configuration. We have found two general types of solutions from the direct calculation of the dispersion relation for both configurations. The two solutions are the surface or Brewster modes and the virtual modes. The characteristics of both modes are discussed.

The effect of electronic damping upon the dispersion curves for Ag which exhibits low electronic damping and Au which exhibits moderate electronic damping is demonstrated. Finally the perturbing effect of the dielectric (referred herein as dielectric shift) upon the displacement of the dispersion curves to higher wave number for the PAM configuration for Ag and for the PDM configuration for Au is shown.

.../...

I - INTRODUCTION

Many articles [1-12] have been published concerning the determination of the surface plasma wave (SPW) dispersion relation for metals, both theoretical and experimental, from the method of attenuated total reflection (ATR) [1]. The majority of attention has been given to the noble metal Ag because Ag exhibits low electronic damping and therefore large dispersion. Only brief attention has been given to metals with moderate electronic damping such as Au [9,10] or to metals with high electronic damping such as nickel [11,12].

In this study the SPW dispersion curves for Ag as determined from calculated ATR spectra for the PAM configuration and from the direct calculation of the dispersion relation for the same configuration are presented. The SPW dispersion curves for Au have been determined from experimental ATR spectra, from calculated ATR spectra and from the direct calculation of the dispersion relation for the PDM configuration. To our knowledge this is the first reported direct calculation of the dispersion relation for either configuration. We have found two general solutions from the direct calculation of the dispersion relation for both configurations. They are the surface or Brewster modes and the virtual modes as proposed by Kliewer and Fuchs [13,14]. Also we have found that the presence of the dielectric (prism) in proximity to the air-metal surface for the PAM configuration and to the dielectric-metal surface for the PDM configuration causes a shift in the respective dispersion curves to higher wave numbers. We refer to this effect as the "dielectric shift". In effect the dielectric shift is a direct result of the inclusion of the reflection and refraction of the SPW by the second boundary at a finite distance form the metal surface.

In particular we give attention to the effect of the dielectric shift and intrinsic or electronic damping upon the overall shape of the dispersion curve as determined from ATR spectra or a direct calculation of the dispersion relation as derived from Maxwell's equations. Electronic damping is directly

proportional to the magnitude of the imaginary part of the complex dielectric function of the metal. In general, the larger the electronic damping the smaller the SPW dispersion.

The original configuration of the ATR method for inducing and detecting SPW as proposed by Otto [1] is shown in Fig. 1. An alternate arrangement [2] in which the air film is replaced by a thin film of the active medium, i.e., the metal, is shown in Fig. 2. We are concerned only with the original configuration in this study ; the second arrangement will be discussed in a subsequent article.

In section II the two-surface dispersion relation is presented as derived from the electromagnetic wave equation. Comparison is made with published accounts. A discussion of the ATR reflectivity equation is also given. The calculated dispersion curves from the two-surface configuration and from ATR spectra are given in section III with experimental data. Also given in section III is an explicit evaluation of the dielectric shift. A discussion of the results obtained is presented in section IV.

II - THEORY

A) Dispersion relations

The SPW is an electromagnetic wave propagating as a plane wave parallel to the interface of a metal (active medium) and a dielectric but decaying exponentially perpendicular to the interface. The presence of a second dielectric at a distance t from the interface modifies the propagation behavior of the SPW [1]. We show in Fig. 3 the electric fields in the three media configuration.

The three media system consists of a semi-infinite dielectric with dielectric constant ε_o, a dielectric layer of thickness D with dielectric constant ε_1 ($\varepsilon_1 = 1$ for the PAM configuration) and a semi-infinite medium (metal or semiconductor) with a complex dielectric constant $\varepsilon_2 = \varepsilon_{2r} + i\,\varepsilon_{2i}$. The local limit for ε_2 is assumed, i.e.,

$$\varepsilon_2\ (\underline{k},\omega) \rightarrow \varepsilon_2\ (0,\omega)$$

where $\underline{k}$ is the complex wave vector and ω is the real frequency of the optical field

We assume that an evanescent wave has excited the modes of collective oscillation of the electron density at the surface of medium 2. These modes constitute a SPW propagating parallel to the surface in the z - direction but decaying exponentially in the $\pm$x direction. The method of "superposition of waves" is employed to account for waves decaying in both $\pm$ x-directions in medium 1.

From Maxwell's equations, the wave equation that must be satisfied in all three media is, in CGS units,

$$(1) \qquad \nabla(\nabla.\underline{E}_i) - \nabla^2\underline{E}_i - \frac{\omega^2}{c^2}\,\varepsilon_i\,\underline{E}_i = 0 \qquad i = 0,\ 1,\ 2$$

The waves in the three media are transverse magnetic only. SPW in general cannot be transverse electric waves. In the three medias the electric fields are

$$(2) \qquad \underline{E}_0 = \left(-\frac{k^2}{\alpha_0},\ 0,\ i\,k\right)\underline{E}_{0p}\ e^{-\alpha_0 x}$$

$$\underline{E}_1^{\pm} = \left(\pm \frac{k^2}{\alpha_1},\ 0,\ i\,k\right) \underline{E}_{1p}\, e^{\pm\alpha_1 x} \tag{3}$$

$$\underline{E}_2 = \left(\frac{k^2}{\alpha_2},\ 0,\ i\,k\right) \underline{E}_{2p}\, e^{\alpha_2 x} \tag{4}$$

where the decay constants are

$$\alpha_0^2 = k^2 - k_0^2\,\varepsilon_0$$

$$\alpha_1^2 = k^2 - k_0^2\,\varepsilon_1$$

$$\alpha_2^2 = k^2 - k_0^2\,\varepsilon_2$$

and

$$k_0 = \frac{2\pi}{\lambda_0} = \frac{\omega}{c}$$

The optical wavelength in vacuum is λ_0. The time and z-dependency factor $e^{i(kz - \omega t)}$ is assumed for all three electric fields. Note that the wave number in the z-direction is simply k.

Applying the appropriate boundary conditions at the two interfaces gives the dispersion relation for SPW propagating parallel to the dielectric-metal surface. The dispersion relation is

$$\frac{\alpha_1\,\varepsilon_2}{\alpha_2\,\varepsilon_1} + \frac{(\varepsilon_0\alpha_1 + \varepsilon_1\alpha_0) + (\varepsilon_0\alpha_1 - \varepsilon_1\alpha_0)\, e^{-2\alpha_1 t}}{(\varepsilon_0\alpha_1 + \varepsilon_1\alpha_0) - (\varepsilon_0\alpha_1 - \varepsilon_1\alpha_0)\, e^{-2\alpha_1 t}} = 0 \tag{5}$$

Note that the second term in Eq. (5) is expressed only in terms of the parameters of the first and second medium, i.e., ε_0, ε_1, α_0 and α_1. For

t very large, the second term is unity and the dispersion relation for a SPW propagating parallel to a dielectric-metal surface obtains

$$k^2 = k_0^2 \left(\frac{\varepsilon_2 \varepsilon_1}{\varepsilon_2 + \varepsilon_1}\right) \tag{6}$$

When t is finite the deviation of the second term in Eq. (5) from unity is a direct measure of the influence of the prism upon the SPW dispersion relation. That is, it is possible to calculate directly the effect of the dielectric shift upon the SPW dispersion curve. Eq. (5) was programmed for computer solution by an iteration technique to yield $k = k_r \pm i\, k_i$. The solution was considered to be acceptable when the magnitude of the argument of the left side of Eq. (5) was less than 10^{-4}.

We have found that the solutions to the dispersion relation, Eq. (5), for the two-surface configuration fall into two classes. The first class is characterized by the decay constant α_0 in the prism having complex values with the imaginary part positive. The real part of α_0 is generally small in magnitude compared to the imaginary part except for very small gap thicknesses at the smaller values of photon energy. The sign of the real part of α_0 is positive for this class of solution except for intermediate values of the gap thickness and certain photon energies where it is negative. The other decay constants α_1 and α_2 are also complex with positive real parts, but the imaginary parts are sometimes positive and sometimes negative depending on the photon energy and the gap thickness. The wave vector k is complex with a positive real part. For some gap thicknesses, particularly at the lower photon energies, the imaginary part of k is found to be negative, although in the limits of infinite gap and zero gap, it is always positive. When the real part of α_0 is positive, this first class of solution corresponds to surface modes of the type discussed by Kliewer and Fuchs [13,14] in which the fields decay exponentially into the inactive medium.

Let us examine the components of the real part of the Poynting vector $\vec{S}$ in the prism which are perpendicular and parallel, respectively, to the interfaces :

$$(7) \qquad \text{Re } S_x = \frac{\omega}{8\pi} \frac{\varepsilon_0 \alpha_{0i}}{|\alpha_0|^2} |E_{0p}|^2 e^{2\alpha_{or} x} e^{-2k_i z}$$

$$(8) \qquad \text{Re } S_z = \frac{\omega}{8\pi} \frac{\varepsilon_0 k_r}{|\alpha_0|^2} |E_{0p}|^2 e^{2\alpha_{or} x} e^{-2k_i z}$$

We see that the component perpendicular to the interfaces is proportional to α_{oi}, the imaginary part of α_0. When α_{0i} is positive, as it is for the case under consideration, there is a flow of energy in the prism toward the active medium. In this sense, the mode is a Brewster mode [20], since there is a single electromagnetic wave in the prism, and it is propagating toward the active medium.

Let us now turn to the second class of solutions to Eq. (5). This class is characterized by the decay constant α_0 having real and imaginary parts which are both negative. The decay constant α_1 has positive real and imaginary parts for the cases studied, whereas α_2 has a positive real part, but either a positive or negative imaginary part depending on the gap thickness and photon energy. The wave vector k has its real and imaginary parts both positive for all cases considered. The values of α_0 for this second class of solution corresponds to the virtual modes of Kliewer and Fuchs [13,14]. The fields increase exponentially going away from the interfaces into the prism, and energy is transported away from the interfaces.

B) Reflectivity equations

The reflectivity equations required to determine the ATR spectra for the prism-dielectric-metal system as shown in Fig. 1 have been discussed exten-

sively in the literature [1-12]. Therefore only the final equations will be presented here.

The simplest set of equations for calculating the ATR spectra is given in terms of a total reflection coefficient R [15] where

$$R = \frac{R_1 + R_2 e^{-i \cdot 2\Delta}}{1 + R_1 R_2 e^{-i\ 2\Delta}} \tag{9}$$

The reflectivity is simply $|R|^2$.

R_1 is the Fresnel reflection coefficient at the prism-dielectric interface, R_2 is the reflection coefficient at the dielectric-metal interface and Δ is the phase factor proportional to the thickness t of the air gap. The Fresnel reflection coefficient R_1 must be modified to yield total internal reflection at the prism-dielectric surface through the application of Snell's law [15].

An alternate form of the total reflection coefficient in terms of the SPW wave vector $\underline{k}$ and the decay constants α_0, α_1 and α_2 of the three media has been given by Otto [6,7]. A third set of equations has been presented by Kaplan et al. [16] in terms of scattering matrices. Both Otto and Kaplan et al. suggest that setting the denominator of their respective total reflection coefficients to zero yields the SPW dispersion relation for a dielectric-dielectric-metal system. Expressions equivalent to Eq. (5) were obtained by so doing. This also served as a check on the validity of the model as shown in Fig. 3.

An equivalence can be shown between Eq. (9) and the total reflection coefficient as presented by Kaplan et al. [16] by using the decay constants expressed in terms of the individual bulk dispersion laws for each medium. The computer calculations of Eq. (9) were tested by programming also the total

reflection coefficient from Kaplan et al. [16]. Identical results were obtained. All calculations of Eq. (9) were performed by varying the angle of incidence by 0.1 degree increments with the photon energy constant. Published optical constants [17] were used in all calculations reported herein. The real part of the surface plasma wave number is given by the relation

$$k_r = k_0 N_0 \sin \phi_0 \tag{10}$$

where ϕ_0 is the angle of incidence for the reflectivity minimum for a constant photon energy and N_0 is the index of refraction of the prism.

III - RESULTS

In the first part of this section we present the SPW dispersion curves for Ag and Au from a direct calculation of the dispersion relation for an air-metal surface, i.e., Eq. (6) to illustrate the dominating effect of electronic damping. In the second part the SPW dispersion curves for Ag for the PAM configuration as calculated from Eq. (5) and Eq. (9) are presented. Finally the SPW dispersion curves for Au for the PDM configuration as calculated from Eqs. (5) and (9) and from experimental results are shown. Experimental results from literature are also included where possible.

The dielectric constants for Ag and Au are plotted as a function of photon energy in Fig. 4. The dispersion curves for Ag and Au as calculated from Eq. (6) are plotted in Fig. 5 for $\epsilon_1 = 1$. It is instructive to compare the magnitude and behavior of $\epsilon_2 = \epsilon_{2r} + i\,\epsilon_{2i}$ for the two metals for E = 2.0 - 4.0 eV with regard to the dispersion relations. For Ag $|\epsilon_{2i}| \ll |\epsilon_{2r}|$ for $E \leq 3.7$ eV.

At E = 3.6 eV ε_{2_r} goes through - 1.0. Then the denominator on the right side of Eq. (6) becomes very small and thus k becomes large. This behavior accounts for the large dispersion for Ag as shown in Fig. 5. The dielectric function of Au does not exhibit this type of behavior and therefore Au does not show large dispersion.

SILVER

The virtual mode (α_{0i} negative) dispersion curves for Ag as calculated from Eq. (5) for gap thicknesses t = 0.2 μm and 0.075 μm are plotted in Fig. 6. The latter thickness was chosen to demonstrate overcoupling. The solid line is the dispersion curve for t = ∞. The dielectric (prism) was Al_2O_3. The dispersion of the index of refraction for Al_2O_3 [18] was included in all calculations. The dispersion curve for t = 0.2 μm is almost identical to that for t = ∞ except in the photon energy range of 2.0 to 3.0 eV where $|\varepsilon_{2_r}| >> 1$. For t = 0.075 μm, the dispersion curve exhibits larger wave numbers and also a larger maximum wave number.

The surface mode (α_{0i} positive) curves for Ag as calculated from Eq. (5) for gap thicknesses t = 0.2 μm and 0.075 μm are plotted in Fig. 7. The curves are very similar to those for the virtual modes - in fact, for t = 0.2 μm they are essentially indistinguishable. For t = 0.075 μm the surface mode curve lies slightly to the left of the virtual mode curve except at the highest photon energies.

The direct calculation of the dielectric shift due to the proximity of the prism, i.e., the second term on the left hand side of Eq. (5), for t = 0.2 μm and t = 0.075 μm for both the virtual mode and the surface mode are shown in

Fig. 8. We see that the deviation of the dielectric shift from unity is larger for the virtual modes than for the surface modes.

The dispersion curves for Ag as determined from the reflectivity minima in calculated ATR spectra are plotted in Fig. 9 for air gap thicknesses t = 0.2 μm and 0.075 μm. The dispersion curve for t = ∞ is plotted for reference. Two dielectric light lines (ϕ_0 = 44.8° and 60.5°) are also shown. For t = 0.2 μm, reflectivity minima can be determined for photon energies ≤ 3.5 eV. For t = 0.075 μm, minima can be determined up to 3.6 eV in the vicinity of which backbending occurs. For t = 0.2 μm, the dispersion curve from reflectivity minima is practically the same as those for both the virtual modes and the surface modes. For t = 0.075 μm, however, the surface mode curve seems to agree slightly better with the reflectivity minima curve than does the virtual mode curve.

GOLD

The PDM configuration for Au was fabricated by vacuum depositing on the base of a 60° heavy dense flint prism first a thin film of MgF_2 (t = 0.065 um) and then a thick film of Au (0.2 μm) at 10^{-7} torr. The ATR spectra were measured in the photon energy range of 1.0 - 2.6 eV. Optical coupling, i.e., a reflectivity minimum, could not be measured above E = 2.6 eV because of the inherent angle of incidence limitation in the reflectometer. The dispersion curve as determined from the ATR spectra is shown in Fig. 10. Also the dispersion curve from the calculated ATR spectra is shown. The dispersion of the indices of refraction [19] of the two dielectrics was included in all calculations. For reference the dispersion curve for a dielectric (MgF_2)-metal configuration as calculated from Eq. (6) is given. Curve fitting of ε_2 to the experimental reflectivity curves, i.e., the ATR spectra was not attempted because of

the close agreement between the two dispersion curves.

The virtual mode (α_{0i} negative) dispersion curve and the surface mode (α_{0i} positive) dispersion curve for Au for the PDM configuration (t = 0.065 μm for MgF_2) as calculated from Eq. (5) are presented in Fig. 11. For reference the dispersion curve from the calculated ATR spectra is also shown. The surface mode dispersion curve is a better approximation to the ATR dispersion curve than the virtual mode dispersion curve at all photon energies. Note that all five dispersion curves exhibit the same general shape, particularly in the photon range of 2.2 - 2.6 eV. This illustrates the dominating effect of the moderate electronic damping of Au.

The real and imaginary parts of the SPW number for Au are listed in Tables 1 and 2 for E = 1.14 eV and E = 2.26 eV respectively for the virtual mode, the surface mode and from ATR spectra for several dielectric film thicknesses. The imaginary part k_i was calculated from the ATR spectra using the relation

$$k_i = k_o No \cos\phi_M \Delta\phi \tag{11}$$

where ϕ_M is the angle of incidence at the reflectivity minimum and $\Delta\phi$ is the half-width at half-minimum of the reflectivity curve. The two photon energies were selected to illustrate the difference in values of k close to the dielectric light line, i.e., at E = 1.14 eV and far from the dielectric light line, i.e., at E = 2.26 eV. As shown in Table 1 detectable ATR coupling begins at t = 2.25 μm. At t = 2 μm, k for both the surface mode and virtual mode agree with k from ATR spectra. However at t = 1 μm k_i for the surface mode is negative and becomes more negative as t decreases to t = 0.065 μm. At t = 0.065 μm k_i is smaller in magnitud as is k_i for the virtual mode and ATR spectra. This decrease in magnitude indi-

cates the strong overcoupling that occurs between t = 0.1 μm and t = 0.065 μm.

Detectable ATR coupling begins at t = 0.25 μm for E = 2.26 eV as shown in Table 2. At this dielectric film thickness k_r is larger for both modes than k_r for ATR spectra but k_i is smaller for both modes than for ATR spectra. For the surface mode k_i decreases monotonically but dues not become negative. The surface mode is a better aproximation to the ATR spectra than the virtual mode as can be seen by comparing the values of k_r for all film thicknesses.

The direct calculation of the dielectric shift from Eq. (5) is shown in Fig. 12 as a function of photon energy for both the virtual mode and the surface mode. Note the large deviation from unity in the lower photon energy range where $|\varepsilon_{2r}| >> 1.0$ (cf. Fig. 4). In Fig. 13 the dielectric shift is plotted as a function of dielectric film thickness for E = 1.14 eV and 2.26 eV for both the virtual and surface modes. Note that the deviation from unity is more nonlinear and begins at a greater film thickness at E = 1.14 eV than at E = 2.26 eV. Also the dielectric shift is much larger for the lower photon energy. In both

Figs. 12 and 13 the dielectric shift is less for the surface mode than for the virtual mode.

IV - DISCUSSION

We have found that there are two general types of solutions to the dispersion equation for SPW, Eq. (5). These are the surface or Brewster modes, in which the decay constant α_0 in the prism has a positive imaginary part, and the virtual modes, in which α_0 has a negative imaginary part. Both of these modes belong to a group of interface electromagnetic modes which involve a single electromagnetic wave in the prism [20]. The surface mode, which has a positive imaginary part to α_0, involves an electromagnetic wave incident on the prism-air interface, but no reflected wave. This mode is therefore a Brewster-type [20] mode. The virtual mode, on the other hand, has a negative imaginary part to α_0 and therefore involves an electromagnetic wave propagating away from the prism-air interface, but no incident wave. On most of the cases studied in the present work the imaginary part of α_0 is larger in magnitude than the real part for both the surface and virtual modes. Consequently, these modes possess more of a propagating than a decaying character in the prism.

Let us discuss for a moment the virtual mode solutions. The real part of α_0 is negative, so the fields increase exponentially going away from the interfaces into the prism, and energy is transported away from the interface. As pointed out by Kliewer and Fuchs [13] one should introduce a complex frequency which will lead to a temporal decay of the wave and which will compensate for the exponential growth with distance into the prism. Another point which should be mentioned is the increase in value of k_i as the air gap thickness is decreased

from large values. As the coupling to the prism increases through the reduction in gap thickness, the rate of energy transport away from the interfaces increases, and the wave must therefore decay more rapidly in the direction of propagation. Although this behavior was observed for most values of photon energy, it was not found at the highest photon energies where backbending occurs.

Now let us turn to the surface or Brewster modes. In this case the value of k_i decreases as the air gap thickness decreases from large values. The flow of energy in the prism is toward the interface and increases as the gap thickness decreases. This flow of energy into the interface region tends to offset the decay of the mode due to the intrinsic damping in the active medium ; hence, k_i decreases. For some gap thicknesses and some photon energies, the value of k_i is negative. On the face of it, this would imply amplification of the wave. However, there is no mechanism available for amplification. A possible way of resolving this situation is to invoke a complex frequency so that the temporal decay of the wave thereby introduced will offset the spatial growth of the wave.

ACKNOWLEDGEMENT

We would like to thank Dr. G. CHAUVET, Mr. J. LANIRAY and Mr. G. SAURON for their assistance in constructing the reflectometer and Dr. D. ZENATTI for the preparation of the PDM-Au sample.

.../...

TABLES

TABLE 1 - The real and imaginary parts of k (= k_r + i k_i) for Au are listed for the surface mode, virtual mode and from ATR spectra as a function of dielectric film thickness t at E = 1.14 eV.

TABLE 2 - The real and imaginary parts of k (= k_r + i k_i) for Au are listed for the surface mode, virtual mode and from ATR spectra as a function of dielectric film thickness t at E = 2.26 eV.

TABLE I

t	SURFACE MODE		VIRTUAL MODE		ATR SPECTRA	
	k_r	k_i	k_r	k_i	k_r	k_i
2 μm	0.808	0.001	0.808	0.001	0.808	0.001
1 μm	0.806	- 0.001	0.806	0.004	0.806	0.004
0.5 μm	0.801	- 0.021	0.802	0.025	0.798	0.023
0.2 μm	0.840	- 0.101	0.843	0.105	0.816	0.103
0.1 μm	0.959	- 0.172	0.964	0.178	0.898	0.156
0.065μm	1.106	- 0.163	1.116	0.172	0.997	0.129

ATR coupling begins at t = 2.25μm.

TABLE 2

t	SURFACE MODE k_r	SURFACE MODE k_i	VIRTUAL MODE k_r	VIRTUAL MODE k_i	ATR SPECTRA k_r	ATR SPECTRA k_i
0.25μm*	1.855	0.128	1.866	0.137	1.769	0.155
0.2 μm	1.856	0.118	1.882	0.146	1.814	0.143
0.1 μm	1.945	0.050	2.021	0.226	1.939	0.216
0.065μm	2.085	0.040	2.445	0.281	2.082	0.221

* ATR coupling begins at t = 0.25μm.

FIGURES

Fig. 1 - Prism-dielectric-metal system for ATR. At $\phi_o > \phi_c$ (ϕ_c = angle of incidence required for total reflection at the $\varepsilon_0 : \varepsilon_1$ surface) an evanescent wave created at the prism : dielectric surface couples through the dielectric film to excite the SPW at the dielectric : metal surface.

Fig. 2 - Prism-metal-air (PMA) system for ATR. At $\phi_o > \phi_c$ an evanescent wave created at the metal : air surface excites the SPW at the same surface.

Fig. 3 - Schematic diagram showing the configuration of the electric fields in the three media for the derivation of the SPW dispersion relation.

Fig. 4 - Complex dielectric function $\varepsilon_2 = \varepsilon_{2r} + i\varepsilon_{2i}$ versus photon energy E for Ag and Au [17].

Fig. 5 - SPW dispersion curve for gold (——) and silver (---) for a metal-vacuum surface as calculated from published optical data [17] using equation (6) versus photon energy E. The vacuum light line is $k_o = 2\pi/\lambda_o$.

Fig. 6 - Virtual mode dispersion curves for Ag for the PAM configuration for t = 0.2 μm (---) and t = 0.075 μm (—·—) versus photon energy E. The dispersion curve calculated from Eq. (6) (——) and the vacuum light line k_o are also shown.

Fig. 7 - Surface mode dispersion curves for Ag for the PAM configuration for t = 0.2 μm (---) and t = 0.075 μm (—·—) versus photon energy E. The dispersion curve calculated from Eq. (6) (——) and the vacuum light line k_o are also shown.

Fig. 8 - Dielectric shift versus photon energy E for Ag for the virtual mode (——) and surface mode (---) at t = 0.2 μm and 0.075 μm for the PAM configuration.

Fig. 9 - SPW dispersion curves for Ag for the PAM configuration from the calculated ATR spectra for t = 0.2 μm (---) and t = 0.075 μm (—·—) versus photon energy E. The experimental data (x..x) from Otto [1] and two prism light lines (ϕ_o = 44.8°, 60.5°) are shown. The dispersion curve calculated from Eq. (6) is also shown for reference.

Fig. 10 - SPW dispersion curves for Au for the PDM configuration from the experimental (—·—) and the calculated (——) ATR spectra for t = 0.065 μm versus photon energy E. The calculated dispersion curve for t = ∞ (---), i.e., from Eq. (6) (ε_1 for MgF_2) and the dielectric light line k_D are also shown.

Fig. 11 - Virtual mode (—·—) and surface mode (---) dispersion curves for Au for the PDM configuration from Eq. (5) for t = 0.065 μm versus photon energy E. The SPW dispersion curve from the calculated ATR spectra and the dielectric light line k_D are also shown.

Fig. 12 - Dielectric shift versus photon energy for Au for the virtual mode (—·—) and surface mode (---) for the PDM configuration at D = 0.065 μm.

Fig. 13 - Dielectric shift versus dielectric film thickness for Au for the virtual mode (—·—) and surface mode (---) for the PDM configuration at the photo. energies E = 1.14 eV and 2.26 eV.

.../...

REFERENCES

1. A. OTTO,
Z. Physik 216 (1968) 398.

2. E. KRETSCHMANN and H. RAETHER,
Z. Naturforsch. 23A (1968) 2135.

3. E.T. ARAKAWA, M.W. WILLIAMS, R.N. HAMM and R.H. RITCHIE,
Phys. Rev. Letters 31 (1973) 1127.

4. R.W. ALEXANDER, G.S. KOVENER and R.J. BELL,
Phys. Rev. Letters 32 (1974) 154.

5. G.S. KOVENER, R.W. ALEXANDER and R.J. BELL,
Phys. Rev. B14 (1976) 1458.

6. A. OTTO,
Proc. Taormina Conf. on Structure of Matter, Eds. E. Burstein and F. de Martini (Pergammon Press, New York, 1974) 117.

7. A. OTTO,
Optical Prop. of Solids. New Developments (North-Holland, Amsterdam, 1976) 677.

8. R.J. BELL, R.W. ALEXANDER, C.A. WARD and I.L. TYLER,
Surface Science 48 (1975) 253.

9. A.S. BARKER,

Phys. Rev. Letters 31 (1973) 1127.

10. A.S. BARKER,

Phys. Rev. B8 (1973) 5418.

11. P.E. FERGUSON, O.M. STAFSUDD and R.F. WALLIS,

Int. Conf. on Magneto-Optics (Zurich 1976).

12. P.E. FERGUSON, O.M. STAFSUDD and R.F. WALLIS,

Int. Conf. on Magnetism (Amsterdam, 1976).

13. K.L. KLIEWER and R. FUCHS,

Phys. Rev. 153 (1967) 498.

K.L. KLIEWER and R. FUCHS,

Advances in Chem. Phys., Vol. 27, Eds. I. Prigogine and S.A. Rice (John Wiley, N.Y., 1974) 355.

14. R. FUCHS

(Private communication).

15. M. BORN and E. WOLF,

Principles of Optics (Pergammon Press, New York, 1970).

16. H. KAPLAN, E.D. PALIK, R. KAPLAN and R.W. GAMMON,

J. Opt. Soc. Am. 64 (1974) 1551.

17. P.B. JOHNSON and R.W. CHRISTY,
Phys. Rev. B6 (1972) 4370.

18. I.H. KHAN, J.S. LEACH and N.J.M. WILKINS,
Corrosion Science (GB) 6 (1966) 483.

19. The Jean Fichou Company,
94260 Fresnes, France.

20. E. BURSTEIN, A. HARTSTEIN, J. SCHOENWALD, A.A. MARADUDIN, D.L. MILLS and R.F. WALLIS,
Proc. Taormina Conf. on Structure of Matter, Eds. E. Burstein and F. De Martini (Pergammon Press, New York, 1974) 89.

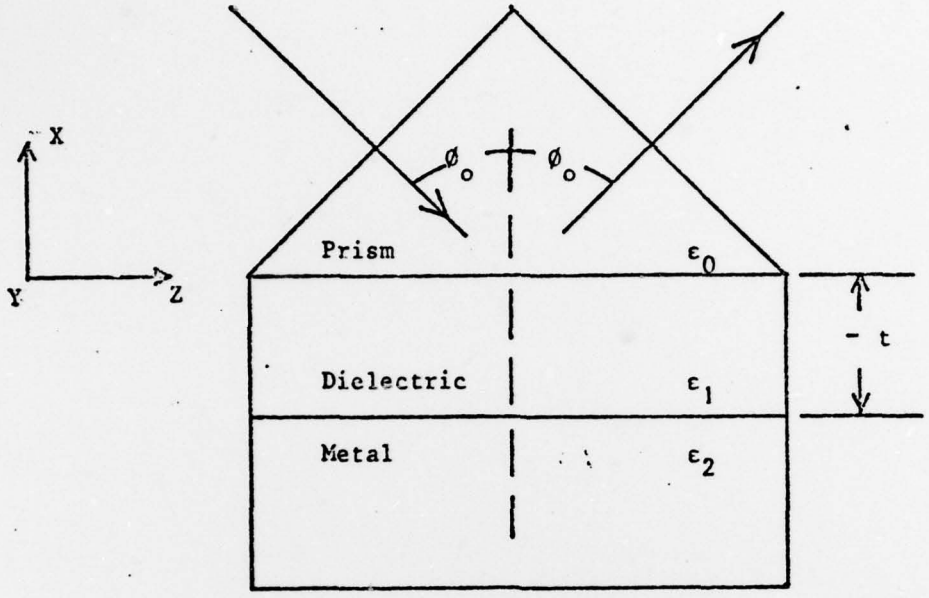
X
Y
Z
ϕ_o
ϕ_o
Prism
ε_0
Dielectric
ε_1
Metal
ε_2
t

Figure 1

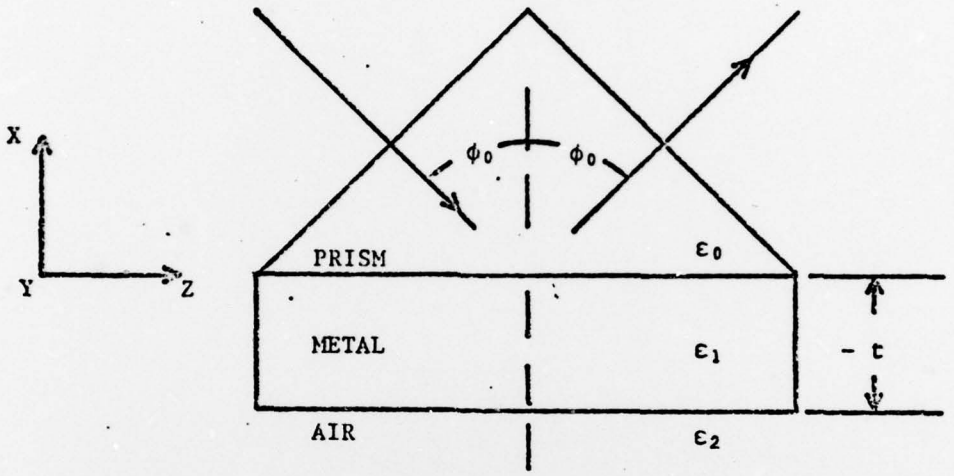
X
Y
Z
ϕ_0
ϕ_0
PRISM
ε_0
METAL
ε_1
- t
AIR
ε_2

Figure 2

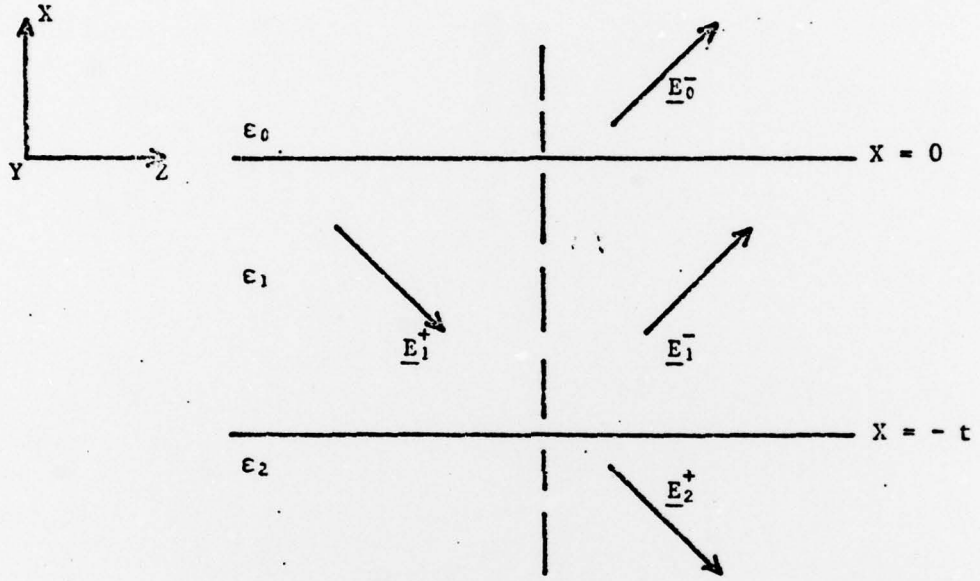
X
Y
Z
ε_0
$\underline{E}_0^-$
X = 0
ε_1
$\underline{E}_1^+$
$\underline{E}_1^-$
X = - t
ε_2
$\underline{E}_2^+$

Figure 3

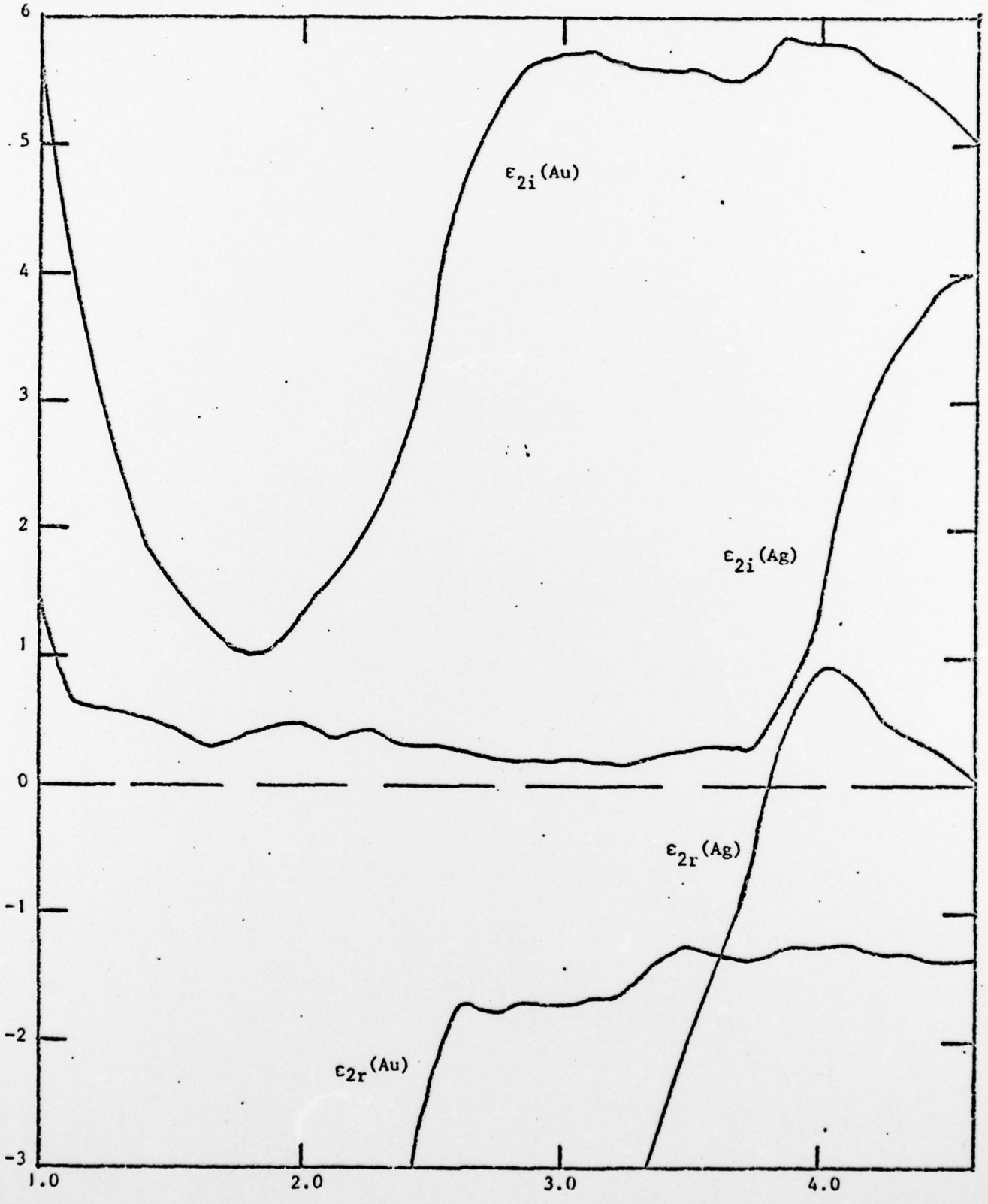
6
5
4
3
2
1
0
-1
-2
-3
1.0
2.0
3.0
4.0
E(eV)
ε_{2i}(Au)
ε_{2i}(Ag)
ε_{2r}(Ag)
ε_{2r}(Au)

Figure 4

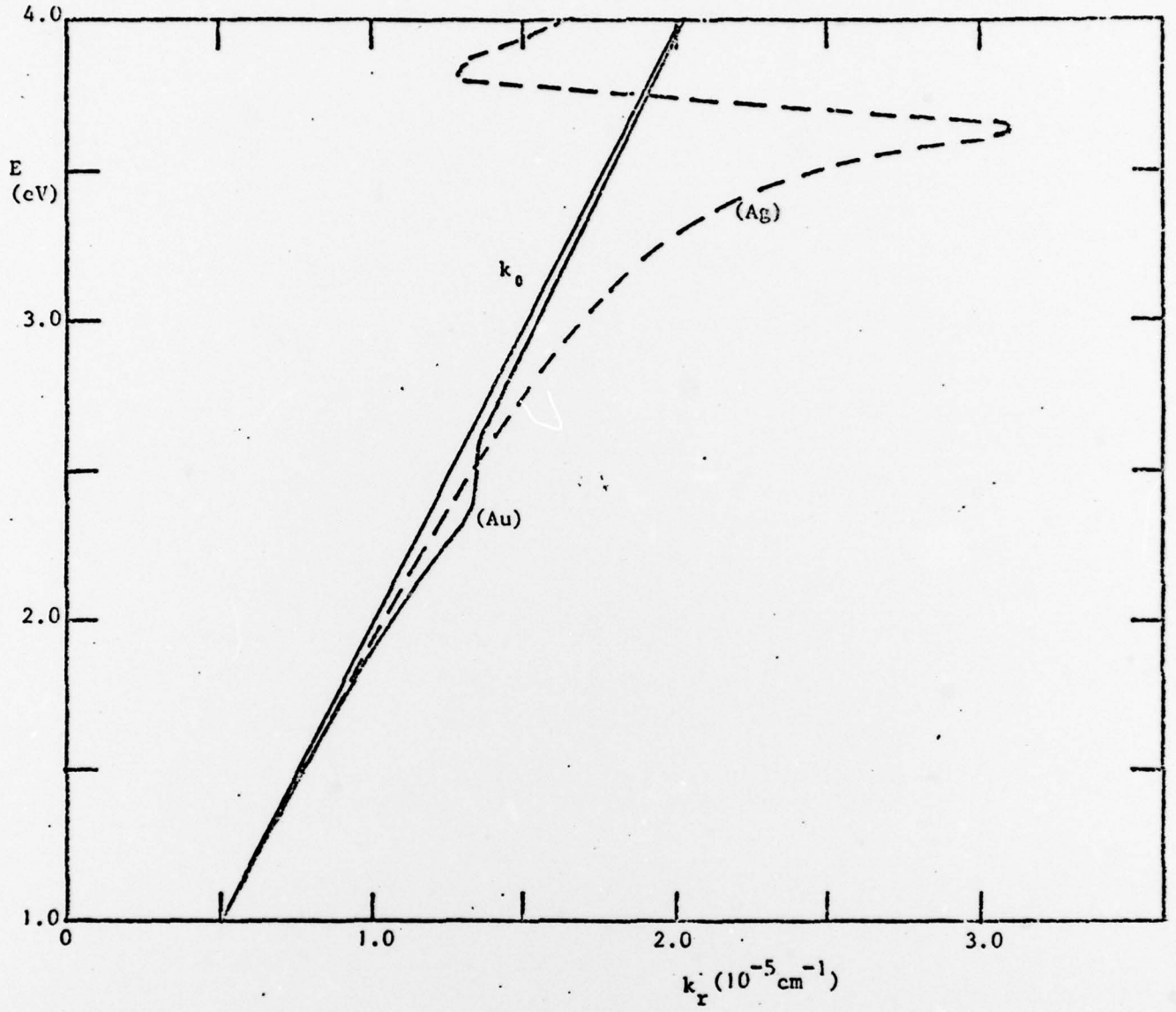

Figure 5

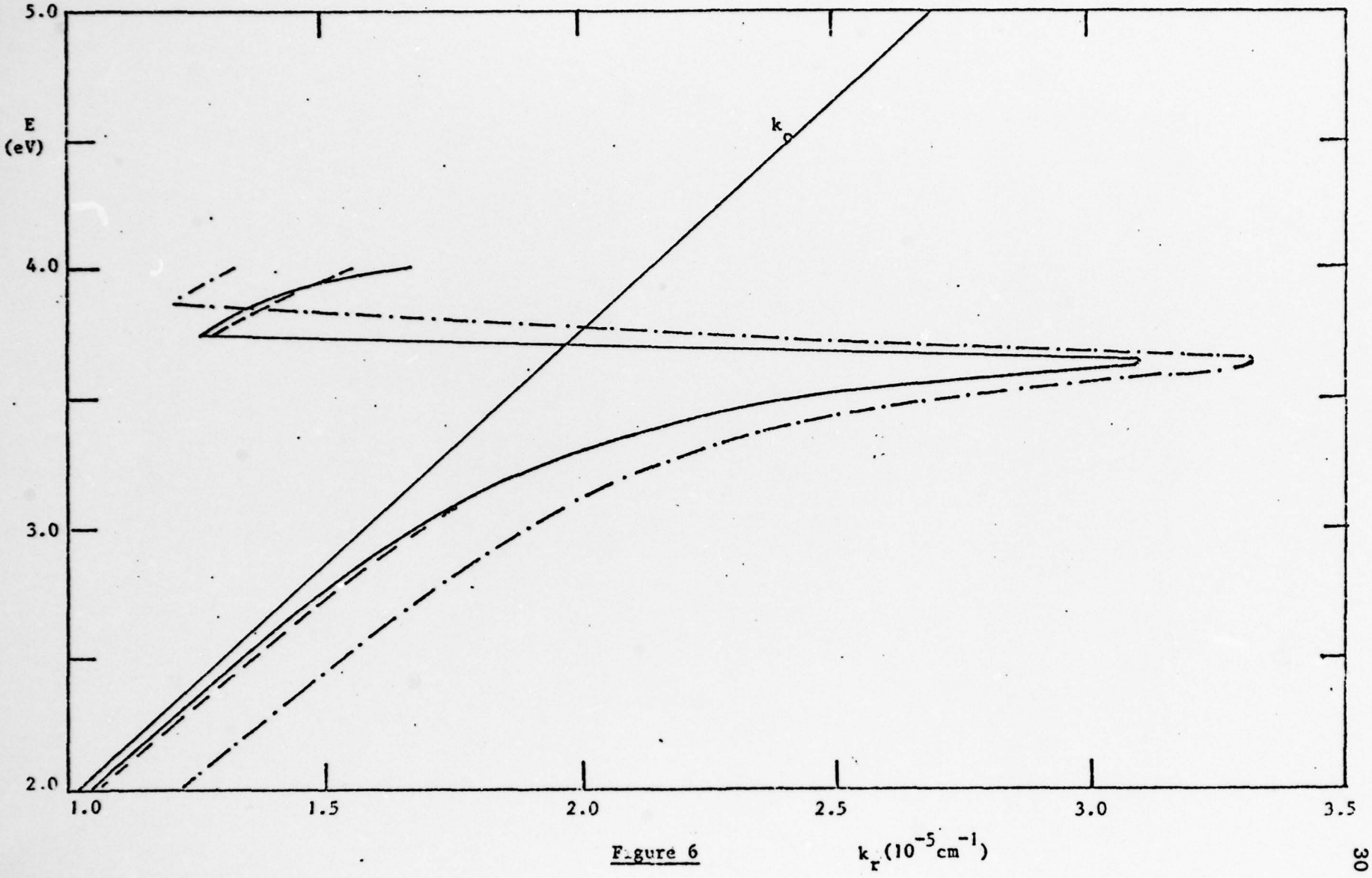

Figure 6

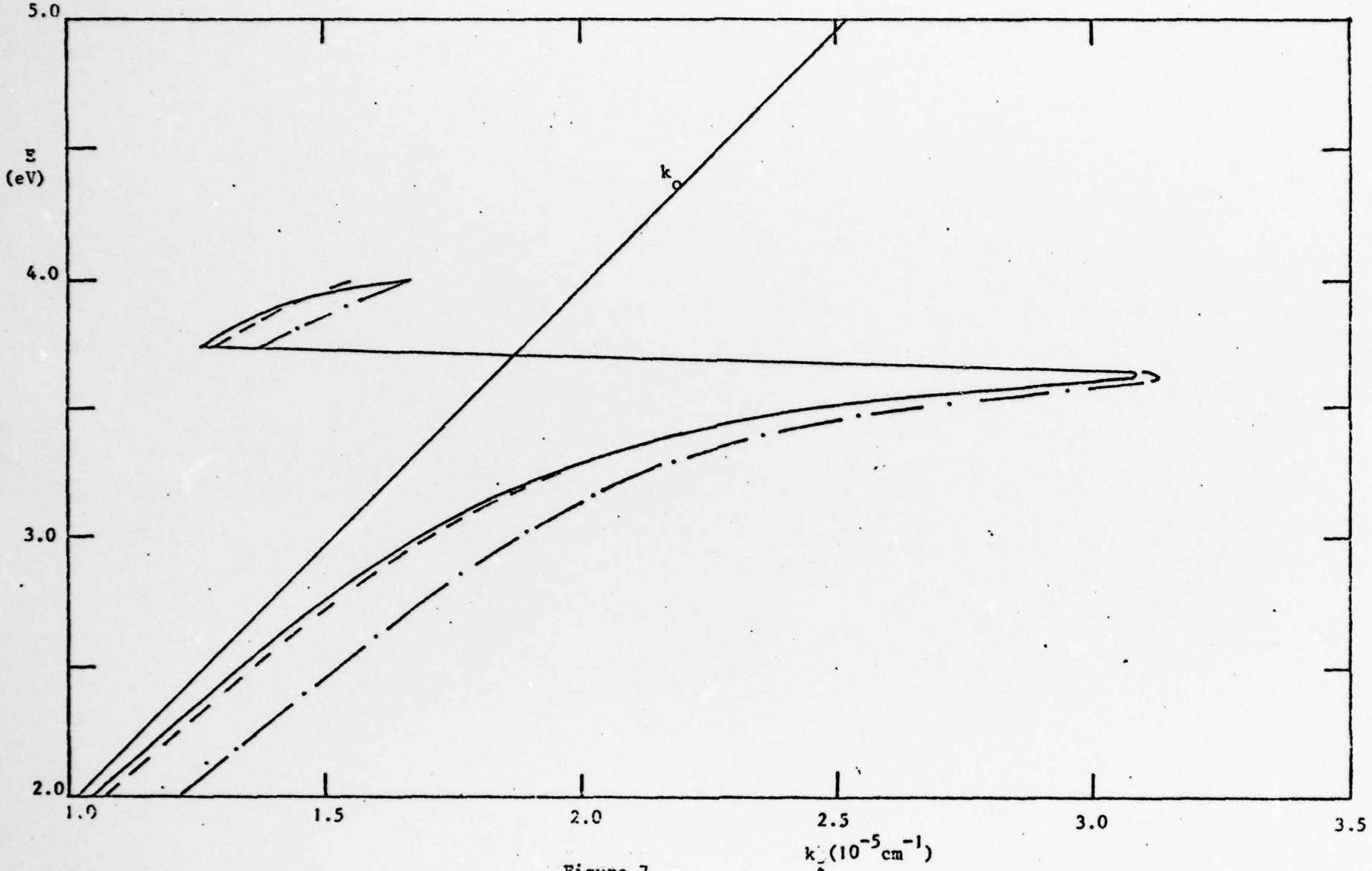

Figure 7

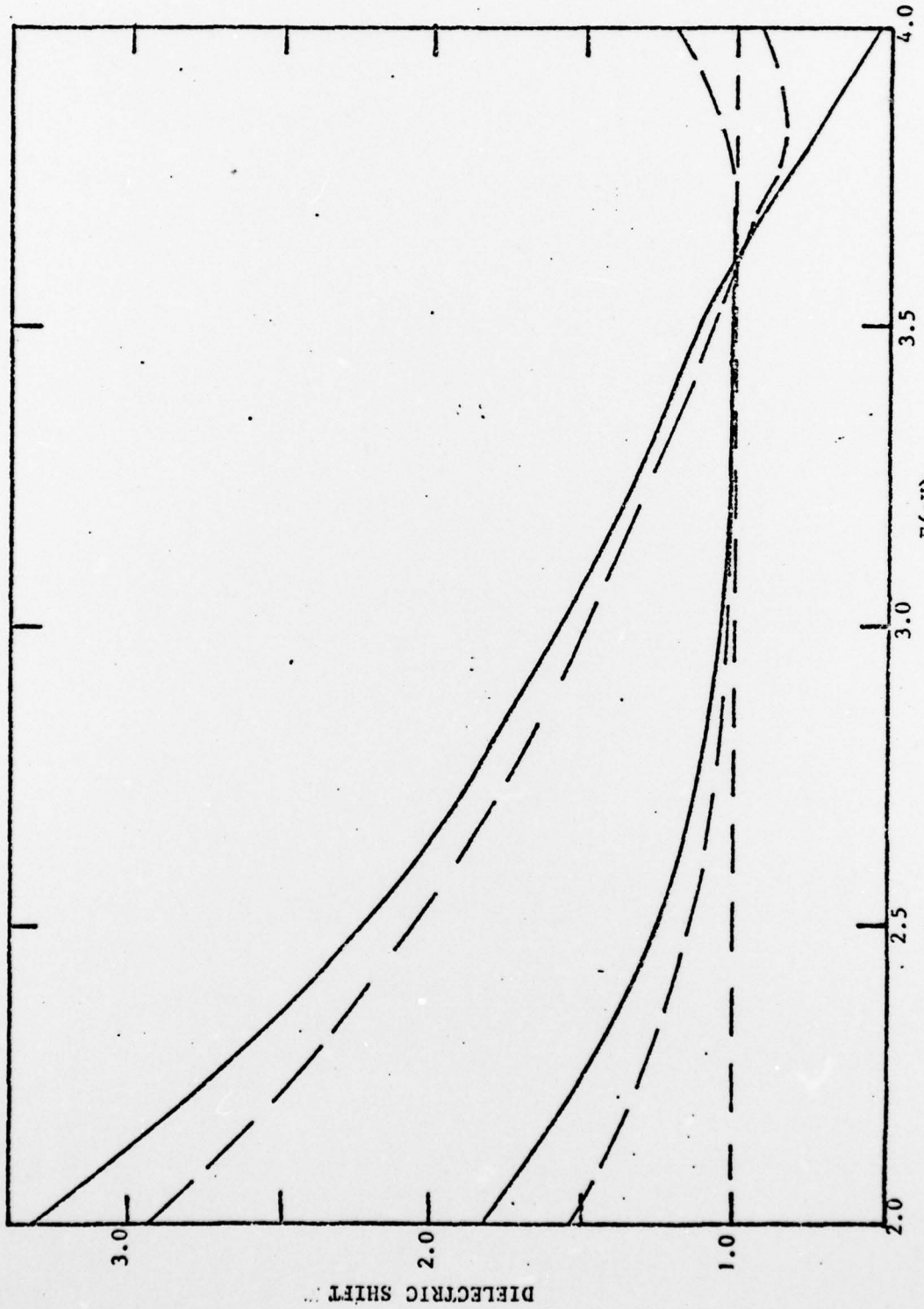

Figure 8

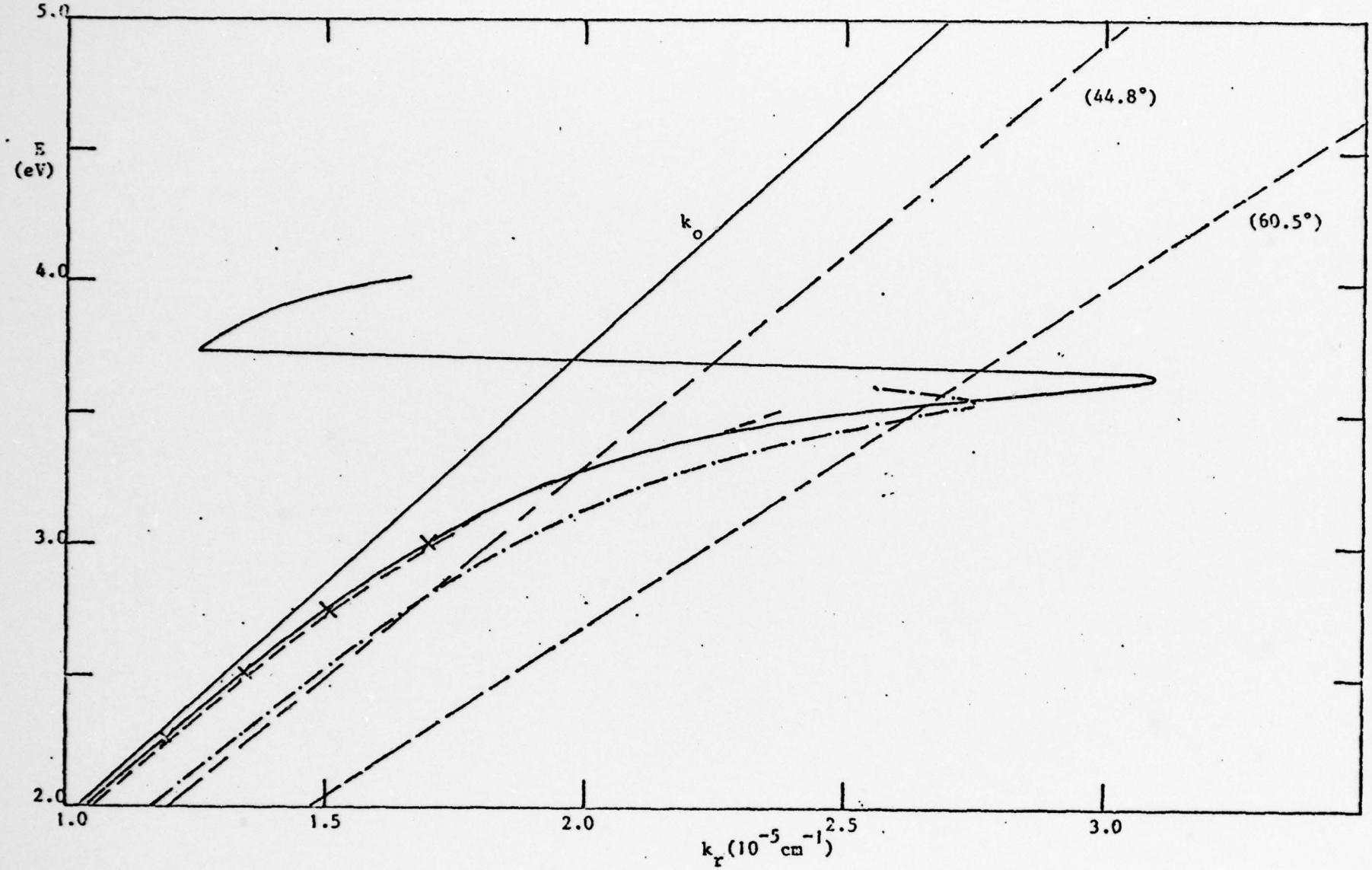

Figure 9

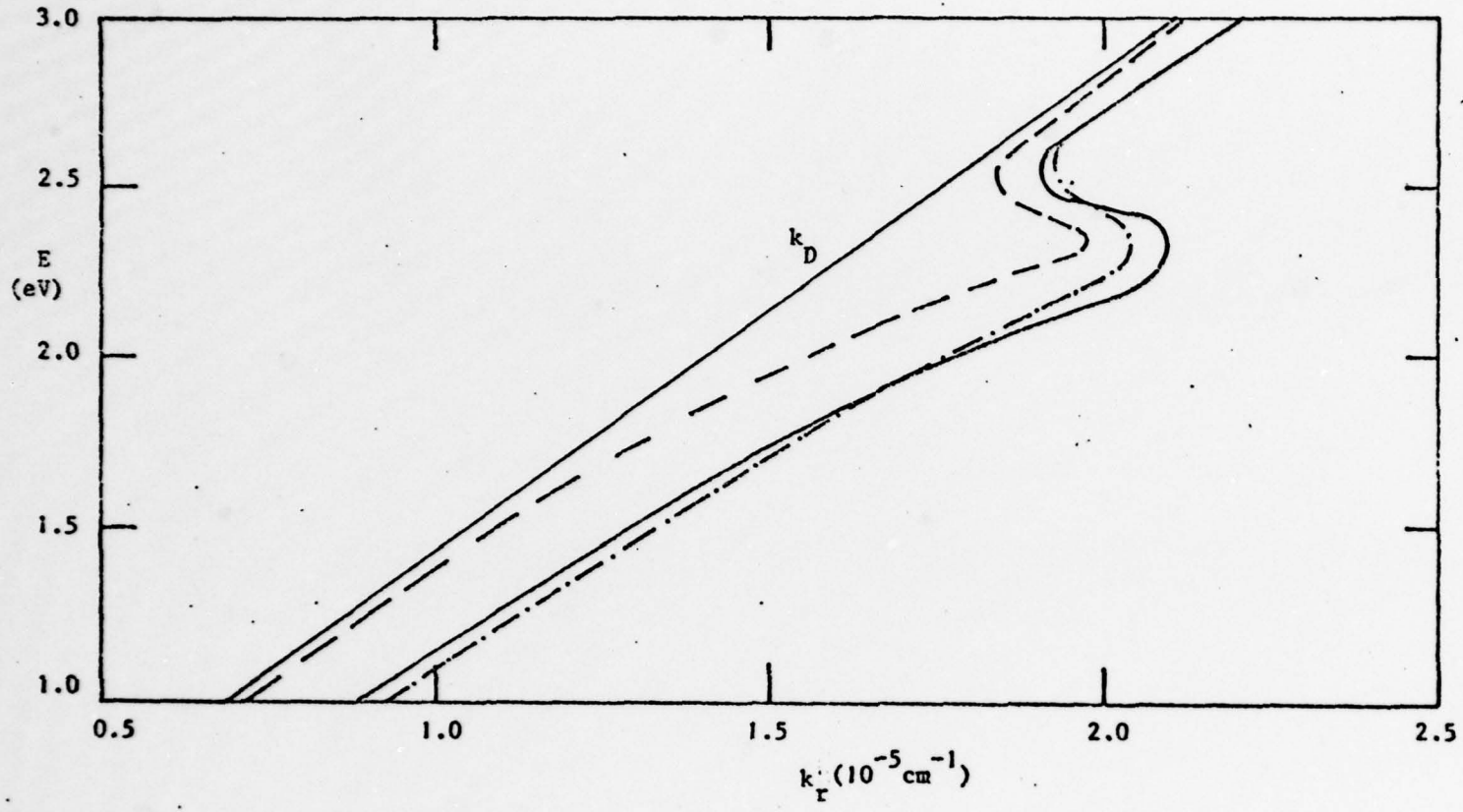

Figure 10

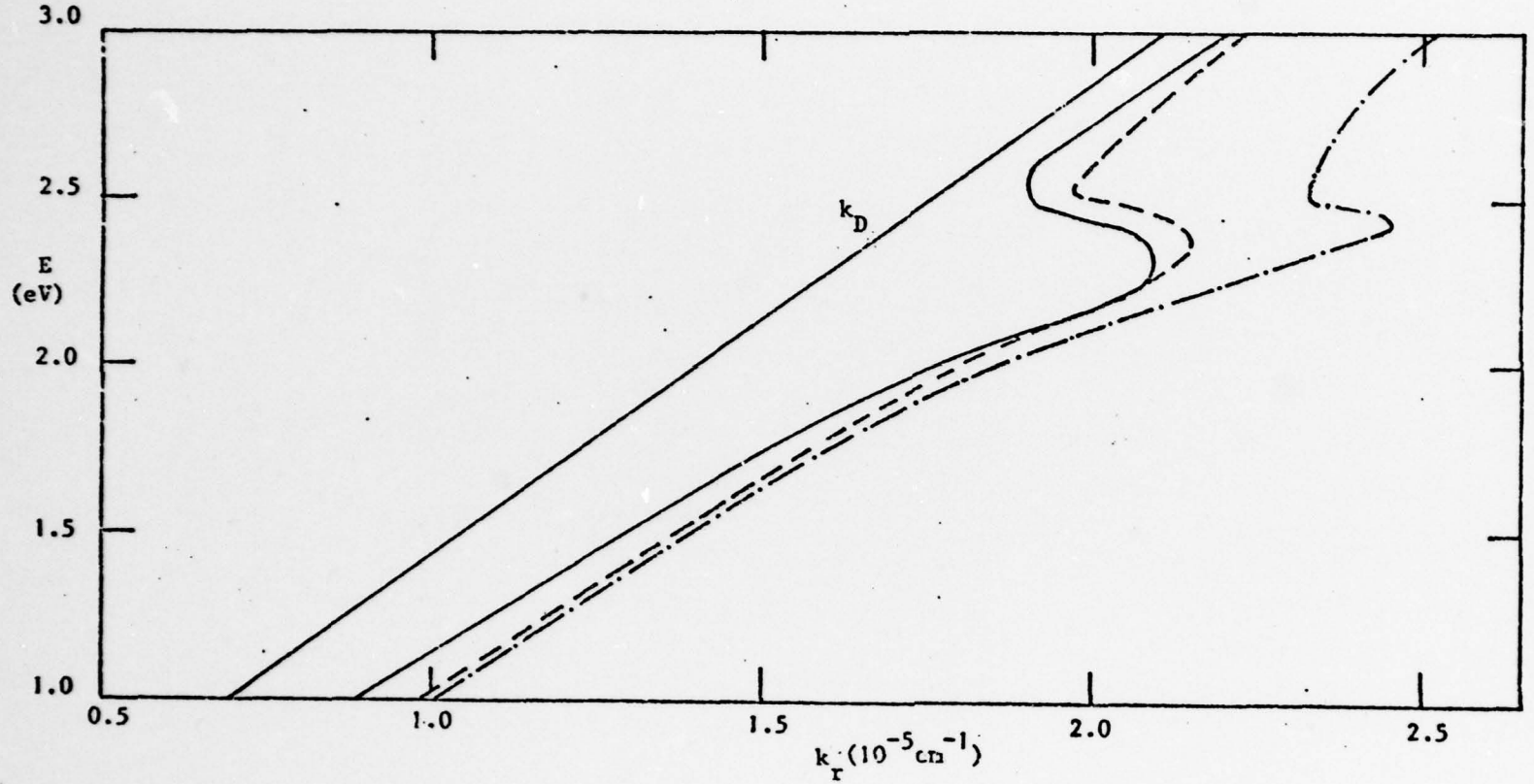

Figure 11

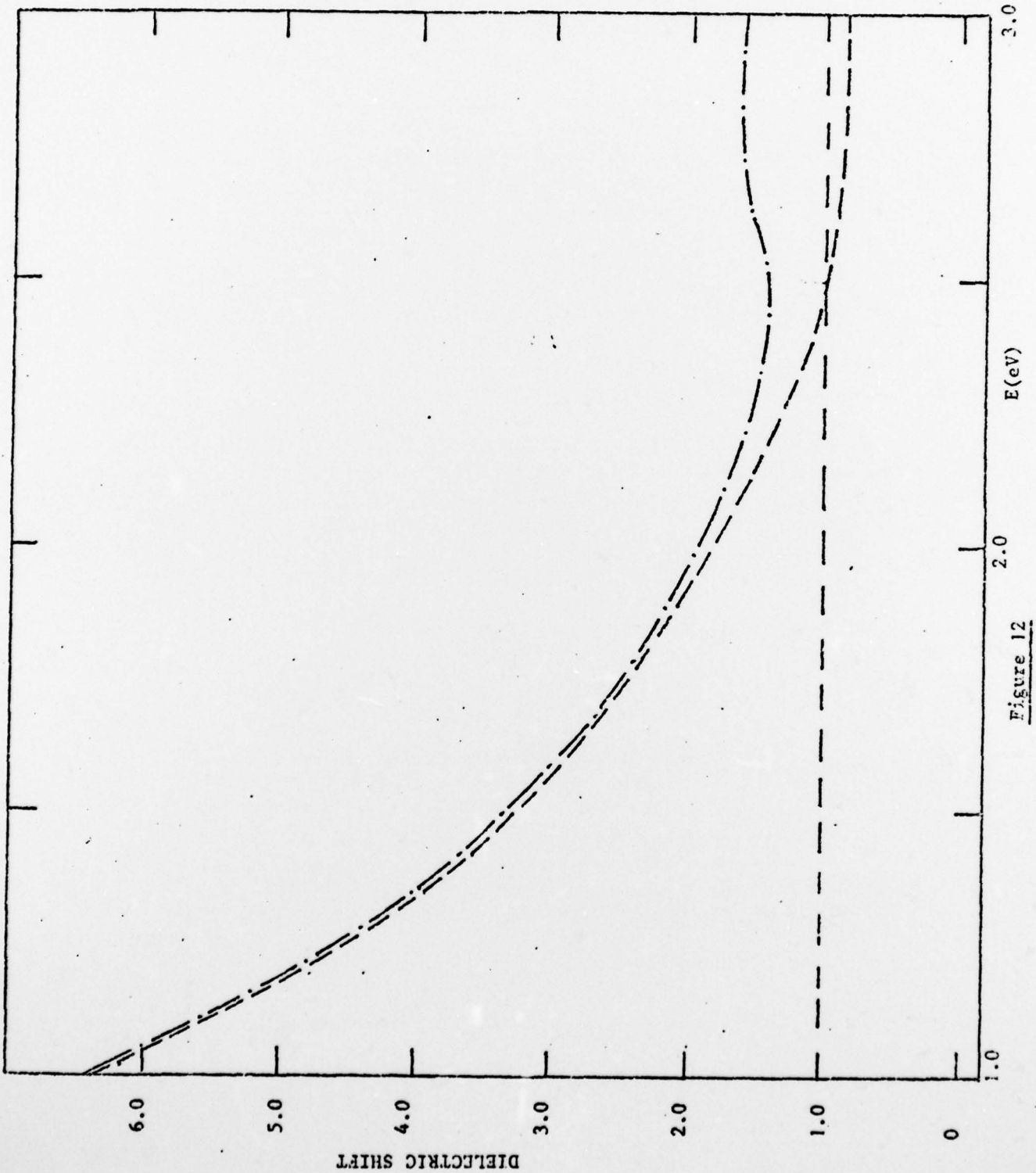

Figure 12

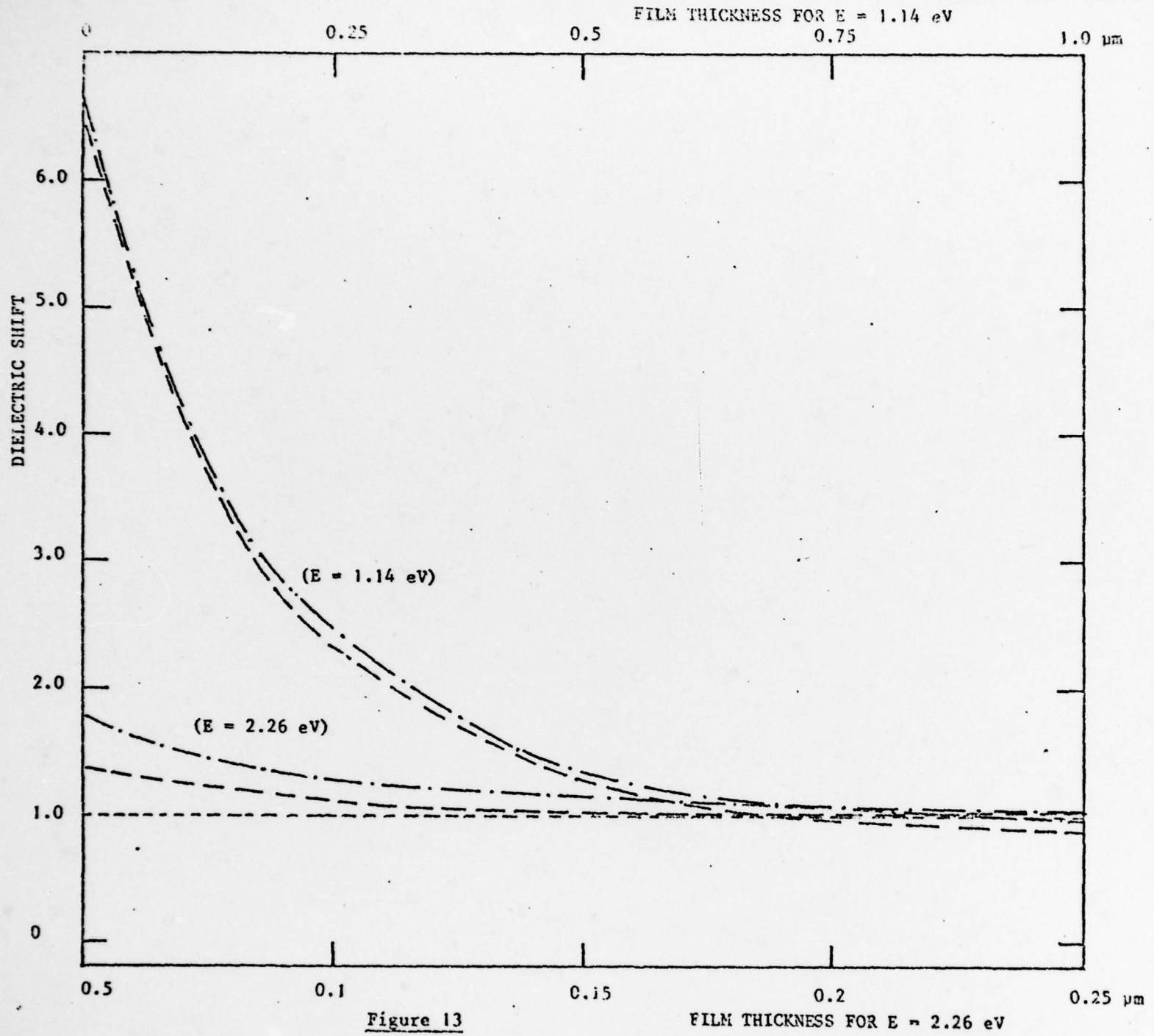
FILM THICKNESS FOR E = 1.14 eV
0
0.25
0.5
0.75
1.0 μm
DIELECTRIC SHIFT
6.0
5.0
4.0
3.0
2.0
1.0
0
(E = 1.14 eV)
(E = 2.26 eV)
0.5
0.1
0.15
0.2
0.25 μm
FILM THICKNESS FOR E = 2.26 eV

Figure 13